# Discrete breathers assist energy transfer to ac-driven nonlinear chains

Danial Saadatmand,[1,*] Daxing Xiong,[2,†] Vitaly A. Kuzkin,[3,4,‡] Anton M. Krivtsov,[3,4,§]
Alexander V. Savin,[5,‖] and Sergey V. Dmitriev[6,7,¶]

[1]*Department of Physics, University of Sistan and Baluchestan, Zahedan, Iran*
[2]*Department of Physics, Fuzhou University, Fuzhou 350108, Fujian, China*
[3]*Peter the Great Saint Petersburg Polytechnical University, Polytechnicheskaya Street 29, Saint Petersburg, Russia*
[4]*Institute for Problems in Mechanical Engineering RAS, Bolshoy pr. V.O. 61, Saint Petersburg, Russia*
[5]*Semenov Institute of Chemical Physics, Russian Academy of Science, Moscow 119991, Russia*
[6]*Institute for Metals Superplasticity Problems RAS, Khalturin 39, 450001 Ufa, Russia*
[7]*National Research Tomsk State University, Lenin Avenue 36, 634050 Tomsk, Russia*

(Received 10 November 2017; revised manuscript received 18 January 2018; published 16 February 2018)

A one-dimensional chain of pointwise particles harmonically coupled with nearest neighbors and placed in sixth-order polynomial on-site potentials is considered. The power of the energy source in the form of single ac driven particle is calculated numerically for different amplitudes $A$ and frequencies $\omega$ *within* the linear phonon band. The results for the on-site potentials with hard and soft anharmonicity types are compared. For the hard-type anharmonicity, it is shown that when the driving frequency is close to (far from) the *upper* edge of the phonon band, the power of the energy source normalized to $A^2$ increases (decreases) with increasing $A$. In contrast, for the soft-type anharmonicity, the normalized power of the energy source increases (decreases) with increasing $A$ when the driving frequency is close to (far from) the *lower* edge of the phonon band. Our further demonstrations indicate that in the case of hard (soft) anharmonicity, the chain can support movable discrete breathers (DBs) with frequencies above (below) the phonon band. It is the energy source quasiperiodically emitting moving DBs in the regime with driving frequency close to the DB frequency that induces the increase of the power. Therefore, our results here support the mechanism that the moving DBs can assist energy transfer from the ac driven particle to the chain.

DOI: 10.1103/PhysRevE.97.022217

## I. INTRODUCTION

For many physical systems, a common basic problem is the response of a nonlinear medium to periodic excitations at the boundary or inside a local region in the bulk [1–11]. The energy can flow or not flow from the energy source into the medium, depending on the medium, the frequency, and the amplitude of the excitations. A linear medium absorbs energy only if the frequency of the source is within the spectrum of small-amplitude running waves (phonons) supported by the medium, while for a nonlinear medium, the energy source can transmit energy into the medium even at driving frequencies outside the small-amplitude phonons spectrum. According to the so-called supratransmission effect [2,12–14], energy, in this case, is transported by the moving discrete breathers (DBs) [15–19] when the driving amplitude is above a threshold value. But some new phenomena beyond the supratransmission effect can also been observed; e.g., for excitation frequencies outside the phonon spectrum, energy can flow into a nonlinear discrete system even at small driving amplitudes [10]; when the system is in contact with heat baths [7], the amplitude threshold for this nonlinear supratransmission effect will be absent.

Recently, interest in the energy transport by linear and nonlinear phonons and by DBs has increased enormously, due to the emerging new field of *phononics* [20,21] and the recent theoretical and experimental progress on anomalous heat transport in low-dimensional systems [22–31], on thermal diodes [32–36], on thermal transistors [37,38], and on various thermal logic gates [39–41]. On the one hand, the relevant theoretical studies showed that DBs [42,43] and solitons [44] can affect thermal conductivity in nonlinear chains. Randomly distributed defects [34,45,46] can also influence heat transport. In particular, the study [47] revealed that heat transport is normal (obeying the Fourier law) in the chains with the interatomic potentials allowing breaking of interatomic bonds. The work [48] suggested the properties of phonon localization and thermal rectification in the chains with strain gradient.

On the other hand, external periodic driving gives new ways in manipulating energy flux in nonlinear lattices. Heat can flow from the low-temperature to the high-temperature heat bath in nonlinear lattices when the temperature of a heat bath is time-periodically modulated [5] or when a driving force with frequency in a certain range is applied at the lattice boundary [7]. An experimental setup for low-frequency phonon cooling with external periodic driving in a diamond nanoresonator has been proposed in [49,50].

In fact, more effort has been devoted to relating the above two aspects. With the time-dependent frequency driving of

*saadatmand.d@gmail.com
†phyxiongdx@fzu.edu.cn
‡kuzkinva@gmail.com
§akrivtsov@bk.ru
‖asavin@center.chph.ras.ru
¶dmitriev.sergey.v@gmail.com

 ©2018 American Physical Society

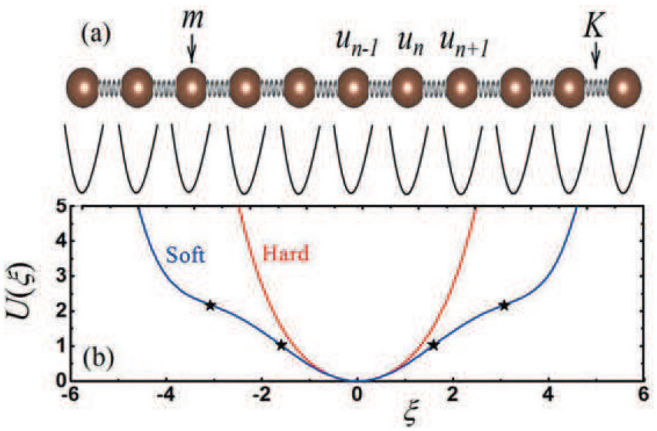


FIG. 1. (a) Schematic plot of the 1D chain of harmonically coupled pointwise particles in the anharmonic on-site potential. (b) The on-site potential as a function of $\xi$ for hard-type (red line) and soft-type (blue line) potentials. The stars show the inflection points in the soft-type case.

a small-amplitude traveling wave, excitation of solitons in the Korteweg–de Vries equation has been analyzed [12]. The possibility of optical excitation of DBs in crystals has also been demonstrated [1]. Excitation of standing DBs with time-modulated vibration amplitude in a strained graphene has been observed [10].

All of the above studies indicate that it is very interesting to study the basic mechanism for energy transfer in nonlinear lattices by external ac driving, and to demonstrate the relevant roles of nonlinear excitations, such as solitons and DBs, within this process. However, so far, the excitation of the latter case, i.e., the DBs, has only been investigated for driving frequencies *outside* the phonon band [2,3,10,12–14]. In this work we therefore study energy transfer in 1D nonlinear chains in the case when the driving frequency is *within* the phonon band.

The rest of this work is composed as follows. In Sec. II the focused 1D nonlinear chains are described, the linear phonon spectrum of these chains is discussed, and the details of our investigation scheme are briefly presented. In Sec. III the energy transfer with a harmonically driven particle in the middle of a linear chain is first analytically demonstrated. Then, numerical results for the chains with hard- and soft-type anharmonicities are given. In Sec. IV the properties of standing and moving DBs in the cases of hard- and soft-type anharmonicities are discussed to explain the findings of Sec. III. Finally, Sec. V draws our conclusions.

## II. MODELS

We consider the 1D chains [see Fig. 1(a)] of pointwise (but with mass $m$) particles whose Hamiltonian is defined by

$$H = \sum_n \left[ \frac{m\dot{u}_n^2}{2} + V(u_{n+1} - u_n) + U(u_n) \right], \tag{1}$$

where $u_n$ is the displacement of the $n$th particle from its equilibrium position, $\dot{u}_n$ is its velocity (the overdot means derivative with respect to time), and

$$V(\xi) = \frac{K\xi^2}{2} \tag{2}$$

is the harmonic potential with stiffness constant $K$ describing the interaction of each particle with its nearest neighbors. For the on-site potential we take

$$U(\xi) = k\xi^2 + \alpha\xi^4 + \beta\xi^6, \tag{3}$$

where $k$ is the coefficient in front of the harmonic term, while $\alpha$ and $\beta$ are the coefficients that define the contributions from the quartic and sixth-order terms, respectively.

Without the loss of generality we set $m = 1$, $K = 1$. Our attention then is focused on the on-site potential, where we take $k = 1/2$ and $\beta = 1/720$. For $\alpha$, we consider the following two cases, i.e., $\alpha = 1/24$ for the hard-type anharmonicity and $\alpha = -1/24$ for the soft-type (only cases for not very large $\xi$ will be taken into account). Thus, in both cases we have unbounded on-site potential, as demonstrated in Fig. 1(b). In fact, for very large $\xi$, both potentials are of hard type since the leading term is proportional to $\xi^6$. As shown in Fig. 1(b), the soft-type potential has four inflection points at $\xi \approx \pm 1.59$ and $\xi \approx \pm 3.07$, which are shown by stars. Therefore, in this study we do not consider excitations with the displacements of particles exceeding the first inflection point to ensure that the anharmonicity of the on-site potential is really of soft type. For displacements exceeding the second inflection point the on-site potential will become effectively harder due to the effect of the sixth-order nonlinear term.

From Eqs. (1)–(3) the following equations of motion can be derived:

$$m\ddot{u}_n = K(u_{n-1} - 2u_n + u_{n+1}) - 2ku_n - 4\alpha u_n^3 - 6\beta u_n^5. \tag{4}$$

As to the case of small-amplitude vibrations, the fourth- and sixth-order nonlinear terms can be neglected, and thus

$$m\ddot{u}_n = K(u_{n-1} - 2u_n + u_{n+1}) - 2ku_n. \tag{5}$$

The solutions of the above equation are the linear combinations of normal modes $u_n \sim \exp[i(qn - \omega_q t)]$ with wave number $q$ and frequency $\omega_q$ following the dispersion relation:

$$\omega_q^2 = \frac{2}{m}[k - K(\cos q - 1)]. \tag{6}$$

In Fig. 2 the dispersion relation (6) is shown within the first Brillouin zone. It suggests that the systems support the small-amplitude running waves (phonons) with frequencies ranging from $\omega_{\min} = 1$ to $\omega_{\max} = \sqrt{5} \approx 2.236$. The phonon group velocity defined by $v_g = d\omega_q/dq$ vanishes for $q \to 0$ and $q \to \pm\pi$, while the phonon with fastest velocity is the one having frequencies in the middle of the phonon band. This fact will be used in the discussion of the power of the energy source.

In simulations we usually consider chains consisting of $N = 4000$ particles. This size is long enough to avoid the effect of boundaries on energy transfer from the driven particle within the simulation run of $t_{\max} = 2000$ time units. The periodic boundary condition is used, i.e., to set $u_n = u_{n+N}$. Equations of motion are integrated with the help of the Störmer method

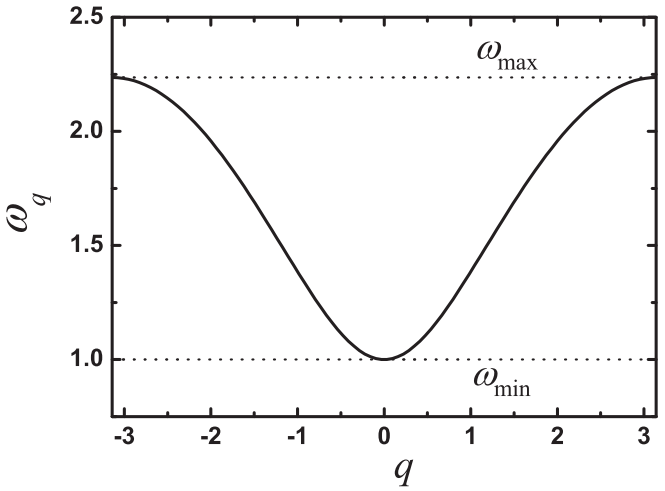


FIG. 2. Dispersion relation for small-amplitude waves (phonons) supported by the considered chain of particles. The phonon band ranges from $\omega_{min} = 1$ to $\omega_{max} = \sqrt{5} \approx 2.236$.

of order six with the time step $\tau = 0.005$. Further decrease of the time step did not affect the final simulation results.

## III. ENERGY TRANSFER TO AC DRIVEN CHAIN

Initially, in the middle of the chain, one particle is forced to move according to the harmonic law

$$u_{N/2} = A\sin(\omega t), \quad T = \frac{2\pi}{\omega}, \tag{7}$$

with the driving parameters, amplitude $A$, frequency $\omega$, and period $T$. All other particles are set with zero displacements and velocities. The driven particle can be regarded as the energy source. The chain can accept or not accept the energy from the source depending on $A$ and $\omega$.

The driving (7) is applied during the whole simulation run up to $t_{max} = 2000$. Such choice of $t_{max}$ ensures that the perturbation from the energy source does not reach the boundaries of the chain for any driving parameters. At the end of the simulation run, we then calculate the total (kinetic+potential) energy $E$ of the chain, and finally find the averaged power of the energy source over the whole simulation runs as follows:

$$P = \frac{E(t_{max})}{t_{max}}. \tag{8}$$

Following this way, the power of the energy source is actually a function of time. To obtain a detailed characteristic of the source power, in practice, we choose to calculate the total energy of the chain $E_j$ at times $t_j = jT$ with $j = 0,1,2,\ldots,$ and $T$ is the driving period. With this information, we then calculate the power averaged over each driving period by

$$p_j = \frac{E_{j+1} - E_j}{T}. \tag{9}$$

### A. Exact solution for driven harmonic chain

Before starting to discuss the nonlinear cases, usually it is very instructive to analyze the behavior of a linear system first [51–55]. In this subsection, we derive an exact expression for the total energy $E$ of the linear system (5) subjected to external excitation (7) under zero initial conditions. This allows us to find both the power $P$ defined by Eq. (8) and the power for each driving period defined in Eq. (9).

To do this we introduce a new variable

$$w_n = u_n - A\sin(\omega t) \tag{10}$$

for convenience. This new variable $w_n$ then satisfies the following equations:

$$m\ddot{w}_n = K(w_{n+1} - 2w_n + w_{n-1}) - 2kw_n + A(m\omega^2 - 2k)\sin(\omega t), \quad w_{\frac{N}{2}} = w_{\frac{3N}{2}} = 0, \tag{11}$$

with initial conditions

$$w_n = 0, \quad \dot{w}_n = -A\omega, \quad n = \frac{N}{2} + 1, \ldots, \frac{3N}{2} - 1. \tag{12}$$

Normal modes for Eqs. (11) are $\sin\frac{\pi j(2n-N)}{2N}$. The corresponding eigenfrequencies are calculated as

$$\Omega_j^2 = \omega_{min}^2 + \frac{2K}{m}\left(1 - \cos\frac{\pi j}{N}\right), \qquad \omega_{min}^2 = \frac{2k}{m}. \tag{13}$$

Therefore, the exact solution of Eqs. (11) can be represented as a linear combination of all normal modes. Including the initial conditions yields

$$w_n = \frac{A}{N}\sum_{j=1}^{N-1} B_j\left[\left(\omega^2 - \omega_{min}^2\right)\sin(\omega t) - \frac{\omega}{\Omega_j}\left(\Omega_j^2 - \omega_{min}^2\right)\sin(\Omega_j t)\right]\sin\frac{\pi j(2n-N)}{2N},$$
$$B_j = \frac{[1-(-1)^j]\cot\frac{\pi j}{2N}}{\left(\Omega_j^2 - \omega^2\right)}. \tag{14}$$

To summarize, formula (14) is the exact solution of Eqs. (11) under initial conditions (12).

Now let us turn to the total energy of the linear system, which is calculated by using the law of energy balance:

$$E(t) = A\omega\int_0^t f(\tau)\cos(\omega\tau)d\tau, \tag{15}$$

where $f$ is the force driving the particle number $N/2$. According to Newton's second law, force $f$ is equal to the difference between acceleration of this particle and forces induced by the neighboring particles and the on-site potential. Then

$$f(t) = A(2k + 2K - m\omega^2)\sin(\omega t) - 2Ku_{\frac{N}{2}+1}. \tag{16}$$

Here the identity $u_{\frac{N}{2}+1} = u_{\frac{N}{2}-1}$ is used. This identity follows from symmetry of the problem with respect to particle number $N/2$.

Next, substituting Eqs. (14) and (16) into Eq. (15) and performing integration yields

$$\frac{E(t)}{A^2} = \frac{1}{2}(2k - m\omega^2)\sin^2(\omega t) - \frac{K}{N}\sum_{j=1}^{N-1} B_j g_j \sin\frac{\pi j}{N},$$
$$g_j = \left(\omega^2 - \omega_{min}^2\right)\sin^2(\omega t) - \frac{2\omega^2\left(\Omega_j^2 - \omega_{min}^2\right)}{\Omega_j\left(\Omega_j^2 - \omega^2\right)}h_j, \tag{17}$$
$$h_j = \Omega_j - \omega\sin(\Omega_j t)\sin(\omega t) - \Omega_j\cos(\Omega_j t)\cos(\omega t),$$

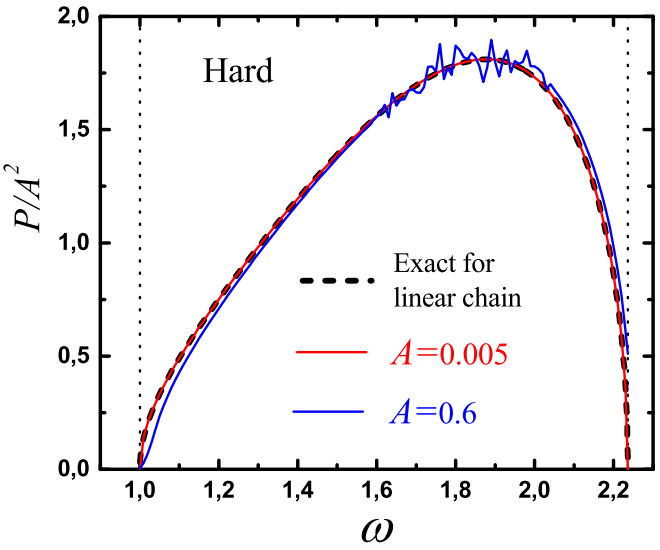


FIG. 3. Power $P$ of the energy source, normalized by $A^2$, as a function of driving frequency for two driving amplitudes, $A = 0.005$ and 0.6. The exact result for the linear chain is shown by the thick dashed line. Vertical dashed lines show the edges of the phonon band with $\omega_{\min} = 1$ and $\omega_{\max} = \sqrt{5}$.

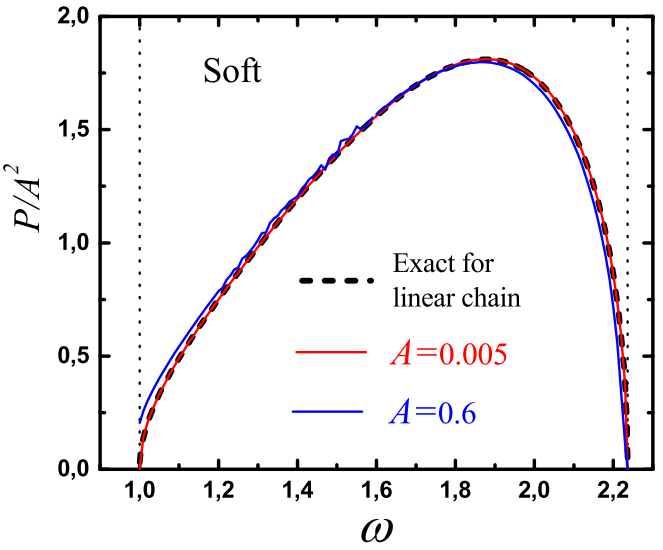


FIG. 4. The same result as that shown in Fig. 3 but for the case of soft anharmonicity.

which is an exact expression for the energy of the linear chain at any moment in time.

Using Eq. (17), one then can calculate both the averaged power of the energy source over time from $t = 0$ to $t = t_{\max}$ and the power for each driving period, based on Eq. (8) and Eq. (9), respectively. For large $N$, the sums in formula (17) can be replaced by integrals. Then applying asymptotic methods, we show that at large times the expression for $E$ has the simple form

$$\frac{E(t)}{A^2} \approx \frac{1}{2} m\omega^2 c_g(\omega) t, \tag{18}$$

where $c_g = \frac{1}{\omega}\sqrt{(\omega^2 - \omega_{\min}^2)(\omega_{\max}^2 - \omega^2)}$ is the group velocity.

Formula (18) has very transparent physical meaning, since $mA^2\omega^2/2$ is the energy density of phonons with amplitude $A$ and frequency $\omega$, while $c_g t$ is the distance traveled by the phonons at time $t$. Thus, the power of the energy source at large times is just a product of phonon energy density and phonon group velocity.

### B. Numerical results for driven nonlinear chain

In Figs. 3 and 4 the power $P$ of the energy source, normalized by $A^2$, is plotted as a function of the driving frequency for two driving amplitudes, $A = 0.005$ and $A = 0.6$, for the hard-type ($\alpha = 1/24$) and the soft-type ($\alpha = -1/24$) anharmonicities, respectively. Driving frequencies are set within the phonon band and marked by the vertical dashed lines. Here, recall that, as mentioned, $P$ is the averaged power over the whole numerical run of $t_{\max} = 2000$. For comparison, the derived exact solution [one can substitute Eq. (17) into Eq. (8)] and some numerical results for several small driving amplitudes are plotted together. For small $A = 0.005$, it can be clearly identified that the numerical results are coincident very well with the prediction. In this case, the normalized power of the energy source is zero at the phonon band boundaries and it has a maximum value $P/A^2 = 1.804$ at $\omega = 1.913$. This can be understood by the fact that the power at large times is proportional to the phonon group velocity, according to Eq. (18), which is zero at the edges of the phonon band and is maximal in the middle of the band.

For the higher driving amplitude $A = 0.6$, the nonlinearity comes into play. So, the results deviate from the prediction of the linear theory. Specifically, for the model with hard-type anharmonicity, $p/A^2$ appears to increase near the upper edge of the phonon band and to decrease near the lower edge, while in the case of soft-type anharmonicity an opposite tendency is observed.

In order to explain this observation, we focus on the driving frequencies within the phonon band but close to its edges. To get deeper insight into the effect of anharmonicity on energy transfer to the chain from the energy source, we plot $p_j$ defined by Eq. (9) as a function of $j$ for a series of driving amplitudes and two driving frequencies $\omega = \omega_{\min} + 0.01$ and $\omega = \omega_{\max} - 0.01$. The results for the hard-type and soft-type anharmonicities are presented in Figs. 5 and 6, respectively, where panel (a) gives the result of driving frequency close to the lower edge of the phonon band, while panel (b) provides that close to the upper edge of the band. The prediction from the linear chain is plotted with the thick dashed line for a comparison. As can be seen, for $A = 0.005$, both the prediction and the simulation results are overlapped as well.

In a detailed comparison of Fig. 5 and Fig. 6, one can easily find that both Fig. 5(a) and Fig. 6(b) show the decrease of the normalized source power with increasing driving amplitude, while a qualitatively different picture is seen in Fig. 5(b) and Fig. 6(a). The former cases are those in which in the lower (upper) edge of the phonon spectrum for hard- (soft-) type anharmonicity, after a transient period, $p_j/A^2$ decreases down to a constant value with the increase of $A$. The latter cases then correspond to those in which, in the upper (lower) edge of the phonon spectrum for hard- (soft-) type anharmonicity, generally $p_j/A^2$ shows not a decrease but an increase with

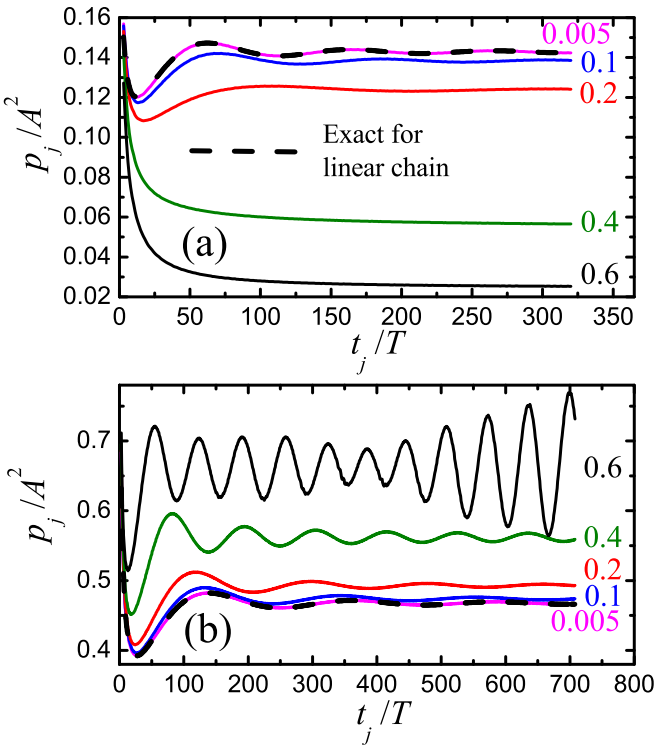


FIG. 5. Hard-type anharmonicity: Power of the energy source $p_j$ defined by Eq. (9) and normalized by $A^2$ as a function of the driving period number, $j = t_j/T$, for different driving amplitudes $A$, as indicated for each curve. Driving frequency is inside the phonon band and it is close to (a) the lower edge, $\omega = \omega_{\min} + 0.01$, and (b) the upper edge, $\omega = \omega_{\max} - 0.01$.

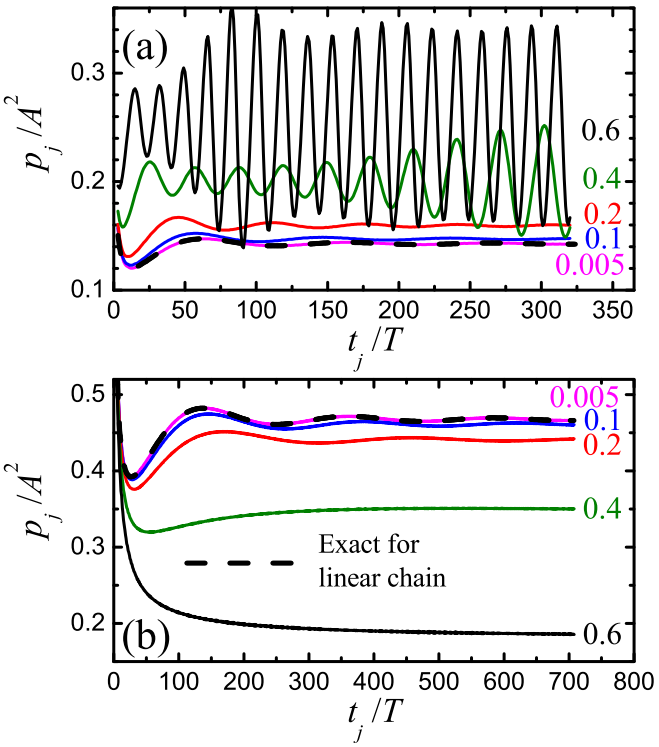


FIG. 6. The same as Fig. 5, but for the case of soft-type anharmonicity.

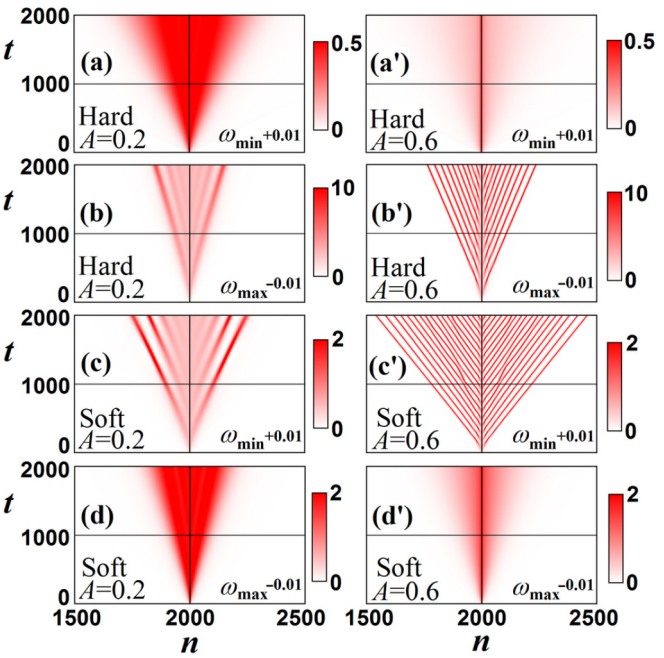


FIG. 7. Contour plots showing the space-time evolution of normalized energy of the particles, $e_n/A^2$. More intense colors correspond to higher energies, according to the color bar shown at the right of each panel. Particle located at $n = 2000$ is driven. (a), (a′), (b), (b′) Hard-type anharmonicity. (c), (c′), (d), (d′) Soft-type anharmonicity. (a), (a′), (c), (c′) Driving frequency is close to the lower edge of the phonon band. (b), (b′), (d), (d′) Driving frequency is close to the upper edge of the phonon band. Left (right) panels correspond to the driving amplitude $A = 0.2$ ($A = 0.6$).

$A$, and more importantly, at large $A$ and a long time, $p_j/A^2$ does not approach a constant value but shows quasiperiodic oscillation behaviors.

The former observations [Fig. 5(a) and Fig. 6(b)] are understandable and trivial, since the driving frequency is close to the edge of the phonon band, while the latter results are interesting, and suggest new underlying mechanisms. Here, we argue that the increase of the power together with quasiperiodic oscillations shown in Fig. 5(b) and Fig. 6(a) at large driving amplitudes is related to excitation of moving DBs, since the driving frequency is close to the DB frequency, while in the cases of Fig. 5(a) and Fig. 6(b), the driving frequency is far from the DB frequency and DBs are not excited, so a qualitatively different picture can be seen. We will present analytic demonstration for the existence of mobile DBs in Sec. IV. Before doing that we first provide more details about the transfer of the energy in the chain to further support the arguments.

The energy per particle is usually defined by

$$e_n = \frac{m\dot{u}_i^2}{2} + \frac{1}{2}V(u_n - u_{n-1}) + \frac{1}{2}V(u_{n+1} - u_n) + U(u_n). \tag{19}$$

In Fig. 7 a contour plot of the normalized (normalized by $A^2$) total energy of all particles (at $n = 2000$, the location of the source), i.e., $e_n/A^2$, during the simulation run up to $t = 2000$ is presented. Here, more intense colors are used to correspond

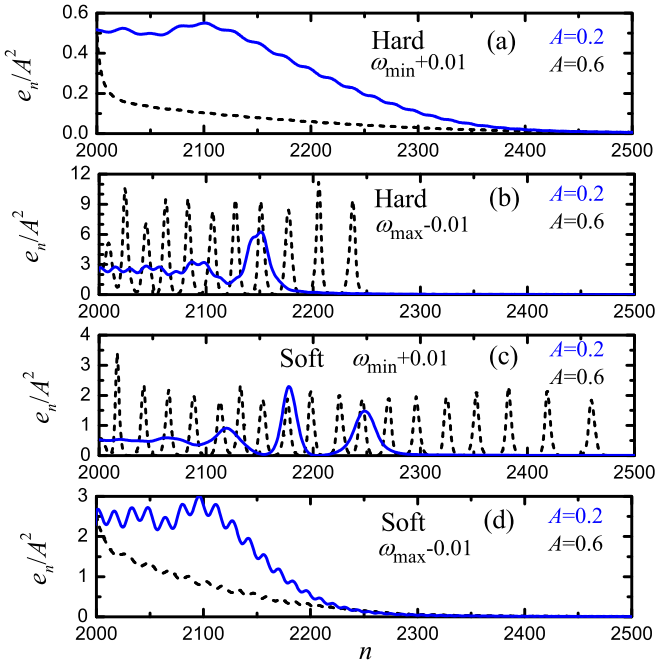


FIG. 8. Normalized energy of the particles at the end of the numerical run at $t = t_{\max} = 2000$. Particle $n = 2000$ is driven. Half of the picture is shown due to the mirror symmetry with respect to the driven site. (a), (b) Hard-type anharmonicity. (c), (d) Soft-type anharmonicity. (a), (c) Driving frequency is close to the lower edge of the phonon band. (b), (d) Driving frequency is close to the upper edge of the phonon band. Blue solid lines show the results of relatively small driving amplitude $A = 0.2$, while black dashed lines correspond to the result of $A = 0.6$, when nonlinearity comes into play. Trains of DBs moving away from the energy source can be seen in (b), (c), when the driving frequency is close to the DB frequency and the driving amplitude is sufficiently large.

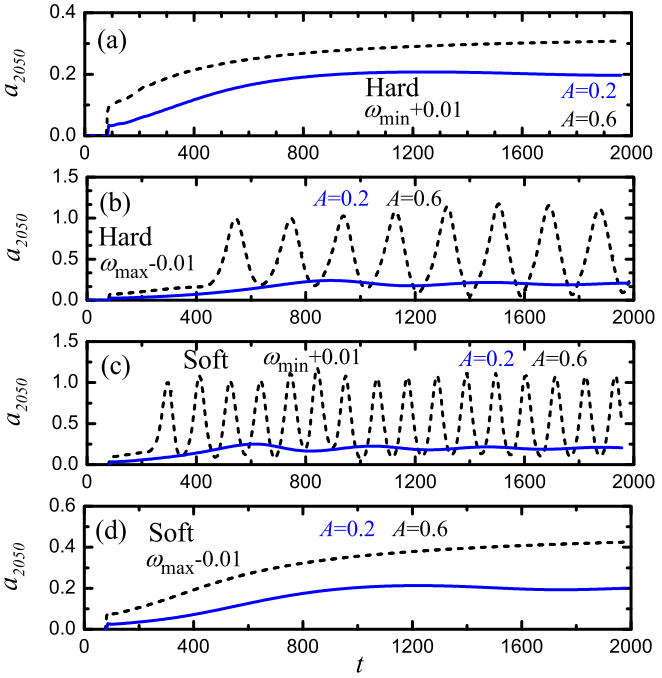


FIG. 9. Vibration amplitude of $n = 2050$ particle as a function of time (driven particle is $n = 2000$). (a), (b) Hard-type anharmonicity. (c), (d) Soft-type anharmonicity. (a), (c) Driving frequency is close to the lower edge of the phonon band. (b), (d) Driving frequency is close to the upper edge of the phonon band. Blue solid (black dashed) lines show the results for $A = 0.2$ ($A = 0.6$).

to the results of higher energy, according to the color bar. The results of the hard-type anharmonicity are presented in panels (a), (a′), (b), (b′), and the counterparts of soft-type anharmonicity are in (c), (c′), (d), (d′). In (a), (a′), (c), (c′) the driving frequency is close to the lower edge of the phonon band, while in (b), (b′), (d), (d′) it is close to the upper edge of the phonon band. Left (right) panels correspond to the driving amplitude $A = 0.2$ ($A = 0.6$).

Indeed, as expected, Fig. 7 shows that the energy flows of panels (a), (a′), (d), (d′) are qualitatively different from those in panels (b), (b′), (c), (c′). This is basically consistent with our above conjecture. In panels (a), (a′), (d), (d′), the normalized energy is better accepted by the chain at *smaller* driving amplitudes, while in panels (b), (b′), (c), (c′) the opposite result is true. In particular, in panels (a), (a′), (d), (d′) the energy radiated by the source is distributed smoothly, while in panels (b), (b′), (c), (c′) the energy distribution is highly nonuniform, which is better seen for larger driving amplitude in panels (b′) and (c′).

We thus present the distribution of $e_n/A^2$ in a more quantitative way. Toward this aim, we show the $e_n/A^2$ simulation run of $t = t_{\max} = 2000$ and plot it in Fig. 8 with panels (a) and (b) hard-type anharmonicity, panels (c) and (d) for soft-type anharmonicity. Recall again that the driven particle is located in the middle of the chain ($n = 2000$), and thus only half of the picture is shown since the energy from the source is emitted symmetrically in both directions, as was evident in Fig. 7. The same as above, in panels (a) and (c) the driving frequency is $\omega = \omega_{\min} + 0.01$, while in panels (b) and (d) it is $\omega = \omega_{\max} - 0.01$. In each case the results are compared for the relatively small driving amplitude $A = 0.2$ (blue solid line) and sufficiently large driving amplitude $A = 0.6$ (black dashed line), where the effect of nonlinearity becomes noticeable (see also Figs. 5 and 6).

For the driving frequency far from the DB frequency [see Figs. 8(a) and 8(d)] $e_n/A^2$ is larger for smaller $A$, in line with the results shown in Fig. 5(a) and Fig. 6(b). The opposite fact is true for the driving frequency close to the DB frequency [see Figs. 8(b) and 8(c)], as was already concluded in Fig. 5(b) and Fig. 6(a).

More interestingly, in the case of the driving frequency close to the DB frequency, we almost recover the quasioscillation behavior shown in Fig. 5(b) and Fig. 6(a). In this case, the energy distribution is in the form of a series of peaks corresponding very similarly to a train of moving DBs emitted by the energy source. Regarding the difference between the results of Figs. 8(b) and 8(c), we point out that this may because DBs emitted at driving amplitude $A = 0.6$ propagate faster than the small-amplitude waves emitted at $A = 0.2$.

To gain clearer evidence, we further analyze the vibration amplitude of one particle located at $n = 2050$, which is 50 sites away from the energy source. The vibration amplitude, $a_{2050}$, as a function of time is presented in Fig. 9, where the relevant

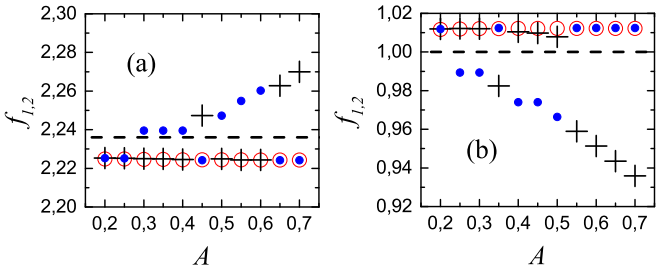


FIG. 10. The associated frequencies of the vibrations shown in Fig. 9 as a function of the driving amplitude $A$. Here we use the open circles to represent the estimated frequencies within the phonon band, while adopting the crosses and dots to denote those that can appear outside the phonon band. Therefore, in (a) [(b)] the open circles (the crosses and dots) are for the soft- (hard-) type anharmonicity.

parameters are the same as those in Fig. 8. From Fig. 9, for small driving amplitude, e.g., $A = 0.2$, the results are similar regardless of which types of anharmonicity and what values of the driving frequency. In all four cases, as time grows, $a_{2050}$ approaches the driving amplitude. This can be understood by the picture that, at small driving amplitudes, the source emits phonons with the amplitude equal to the driving amplitude, whereas the results for the larger driving amplitude, e.g., $A = 0.6$, are sensitive to the parameters. When the driving frequency is far from DB frequencies [Figs. 9(a) and 9(d)], $a_{2050}$ increases with time monotonically, while for the driving frequency close to the DB frequencies, it is oscillated in time since energies are carried by DBs passing quasiperiodically through this particle. DB amplitudes in both cases are slightly above 1, which are obviously larger than the driving amplitude.

In view of Figs. 9(b) and 9(c) and to further verify that these oscillations do correspond to moving DBs, we finally calculate their associated frequencies. To do this we first record $u_{2050}(t)$ within $t = 500$ and $t = 1300$; then by a discrete Fourier transform we derive the frequencies $f$. Usually, one can find two frequencies of $f_1$ and $f_2$, corresponding to the main and second maximum from the spectrum, respectively (if the second maximum is presented). Figure 10 shows the frequencies as a function of the driving amplitude $A$. Here we use the horizontal dashed lines to denote the edges of the phonon band. Figure 10(a) is used to demonstrate our conjecture in Figs. 9(b) and 9(d), where for the soft-type anharmonicity (open circles), its frequencies have only single maximum $f_1$ within the phonon band, whereas for the hard-type anharmonicity (crosses and dots), both $f_1$ (crosses) and $f_2$ (dots) can be observed. In particular, in the latter case, for $A < 0.3$, one only sees the frequencies within the phonon band, while for $A \geqslant 0.3$, the frequencies above the phonon band can be clearly identified. In Fig. 10(b), a similar behavior can be seen, but now we focus on the soft-type anharmonicity case and with the frequencies below the linear phonon band [see the crosses and dots in Fig. 10(b)].

From Fig. 10 now we confirm that, by driving with frequency within the phonon band, one can produce vibrations of additional frequencies outside the band. Clearly, such frequency regimes just correspond to the DB frequencies outside the linear phonon band, for the hard- and soft-type anharmonicities, respectively. This evidence thus further supports that the oscillations shown in Figs. 9(b) and 9(c) just correspond to moving DBs.

## IV. DISCRETE BREATHERS

We now provide information on DBs. We will first numerically explore the properties of standing DBs and then consider their mobility. Finally, an analytical result of moving DBs is presented for comparison.

### A. Standing discrete breathers

To excite a standing DB, the following ansatz was used for the case of hard-type anharmonicity,

$$u_n(0) = \frac{(-1)^n A_{\mathrm{DB}}}{\cosh[\theta(n - N/2)]}, \quad \dot{u}_n(0) = 0, \tag{20}$$

while for the soft-type anharmonicity, we adopt

$$u_n(0) = \frac{A_{\mathrm{DB}}}{\cosh[\theta(n - N/2)]}, \quad \dot{u}_n(0) = 0. \tag{21}$$

Here $A_{\mathrm{DB}}$ and $\theta$ are the DB amplitude and inverse width, respectively. DB is centered on the middle particle of the chain, $n = N/2$. We stress that Eqs. (20) and (21) are not the exact solutions to Eq. (4), but they produce fairly good initial conditions for DBs. For the chosen $A_{\mathrm{DB}}$, we find $\theta$ by using the trial and error method [56] minimizing the oscillations of the DB amplitude in simulations. After $\theta$ is determined, we then calculate DB frequency, $\omega_{\mathrm{DB}}$, and its total (kinetic plus potential) energy, $E_{\mathrm{DB}}$. These results are presented in Table I for a set of DB amplitudes for both hard- and soft-type anharmonicities.

Table I tells us that, with the increase of DB amplitude, the degree of its spatial localization, characterized by $\theta$, increases. The same is true for DB energy, while DB frequency increases (decreases) with amplitude being above (below) the phonon band for hard-type (soft-type) anharmonicity.

Based on Table I, Fig. 11 further plots several typical DB profiles for hard-type [see Fig. 11(a)] and soft-type [see Fig. 11(b)] anharmonicities. Here, we only plot the DBs at the oscillation phase when particles have largest displacements. A comparison of the results of $A_{\mathrm{DB}} = 0.5$ and $A_{\mathrm{DB}} = 1.5$ indicates that DBs with larger amplitude are more localized. In addition to this common feature, the DB profiles for both types of anharmonicities are different; i.e., in the case of hard-type (soft-type) anharmonicity the DB has a staggered (smooth) shape.

### B. Moving discrete breathers

Moving DBs were excited by using the following physically motivated ansatz [56]. For hard-type anharmonicity, it has the form

$$u_n(t) = \frac{(-1)^n A_{\mathrm{DB}} \cos[\omega_{\mathrm{DB}} t + \delta(n - x_0)]}{\cosh[\theta(n - x_0)]}, \tag{22}$$

while for soft-type anharmonicity it reads

$$u_n(t) = \frac{A_{\mathrm{DB}} \cos[\omega_{\mathrm{DB}} t - \delta(n - x_0)]}{\cosh[\theta(n - x_0)]}. \tag{23}$$

TABLE I. Parameters of standing DB.

| Hard-type anharmonicity | | | |
|---|---|---|---|
| $A_{DB}$ | $\theta$ | $\omega_{DB}$ | $E_{DB}$ |
| 0.5 | 0.126 | 2.240 | 9.954 |
| 0.75 | 0.190 | 2.244 | 14.84 |
| 1.0 | 0.257 | 2.250 | 19.59 |
| 1.25 | 0.326 | 2.259 | 24.27 |
| 1.5 | 0.398 | 2.270 | 28.72 |
| 1.75 | 0.475 | 2.283 | 32.95 |
| 2.0 | 0.560 | 2.299 | 36.75 |
| 2.25 | 0.658 | 2.318 | 39.87 |
| 2.5 | 0.783 | 2.339 | 41.64 |
| 2.75 | 0.933 | 2.369 | 42.59 |
| 3.0 | 1.097 | 2.403 | 43.63 |
| Soft-type anharmonicity | | | |
| $A_{DB}$ | $\theta$ | $\omega_{DB}$ | $E_{DB}$ |
| 0.5 | 0.125 | 0.992 | 1.991 |
| 0.75 | 0.186 | 0.983 | 2.969 |
| 1.0 | 0.246 | 0.969 | 3.928 |
| 1.25 | 0.305 | 0.952 | 4.861 |
| 1.5 | 0.361 | 0.932 | 5.770 |
| 1.75 | 0.414 | 0.908 | 6.656 |
| 2.0 | 0.464 | 0.882 | 7.513 |
| 2.25 | 0.511 | 0.854 | 8.334 |
| 2.5 | 0.551 | 0.824 | 9.170 |
| 2.75 | 0.585 | 0.793 | 10.01 |
| 3.0 | 0.613 | 0.764 | 10.87 |

Here, $\delta$ is a free parameter which characterizes DB velocity, $v_{DB}$, in the case when it is mobile. For example, for $\delta = 0$ the DB velocity is zero, and both Eqs. (22) and (23) essentially reduce to the original ones, Eqs. (20) and (21), respectively. The change of the sign of $\delta$ results in the change of the sign of the DB velocity.

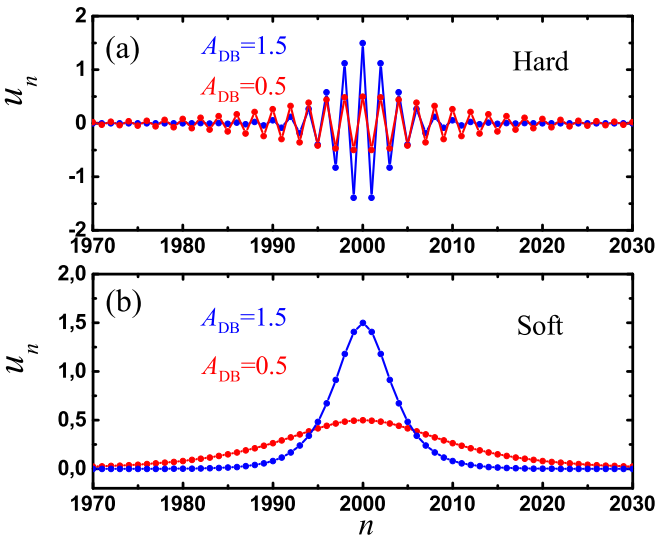


FIG. 11. Standing DB profiles for two different amplitudes $A_{DB} = 0.5$ and $A_{DB} = 1.5$ for the case of (a) hard-type and (b) soft-type anharmonicities.

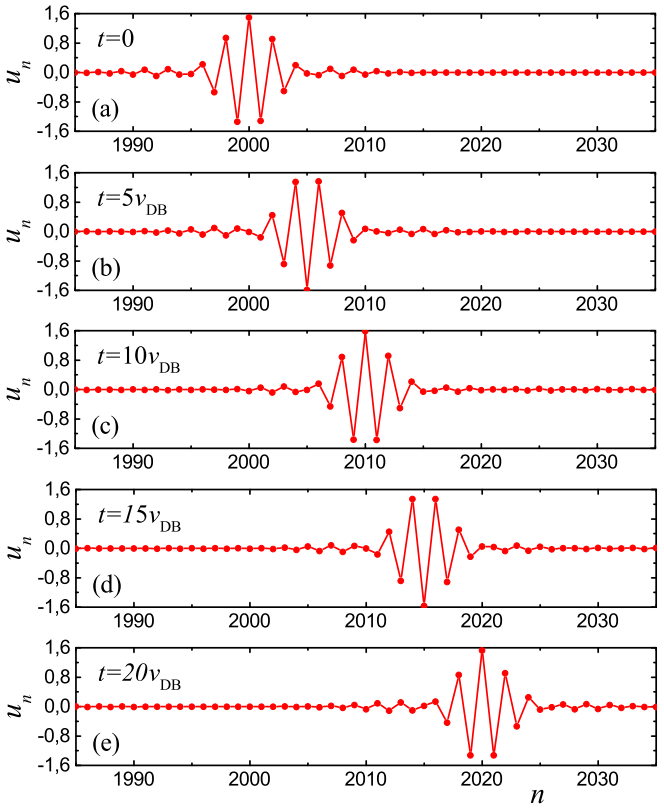


FIG. 12. Moving DB profile in the case of hard-type anharmonicity. Parameters of the ansatz Eq. (22) are $A_{DB} = 1.5$, $\theta = 0.398$, $\omega_{DB} = 2.270$, $x_0 = 2000$, $\delta = 0.3$. DB velocity $v_{DB} = 0.1303$. Time is indicated in each panel.

It should be pointed out that Eqs. (22) and (23) do not describe exact moving DBs, but they give very good approximate solutions for moving DBs in the case of not very high DB amplitude.

We use Eqs. (22) and (23) with different values of $\delta$ for setting the initial conditions taking other DB parameters from Table I. Two typical examples of moving DB evolution are shown in Fig. 12 and Fig. 13 for the hard-type and soft-type anharmonicities, respectively. Here, we choose $\delta = 0.3$, $A_{DB} = 1.5$, $x_0 = 2000$. Other parameters are taken from Table I. The measured DB velocity is $v_{DB} = 0.1303$ in Fig. 12 and $v_{DB} = 0.2838$ in Fig. 13. For these chosen parameters, DBs propagate at constant velocities practically radiating no energy.

The velocity of the DB is measured and presented as a function of $\delta$ in Figs. 14(a) and 14(b) for the chains with hard-type and soft-type anharmonicity, respectively. Different lines show the results for different DB amplitudes, $A_{DB}$, as indicated in the legends.

In fact, in our calculations, we have examined DB velocities for different $A$ in detail. The relevant results are presented in Fig. 14. It can be seen that for hard-type anharmonicity [see Fig. 14(a)], DBs with relatively small amplitudes ($A_{DB} < 2$) have velocities nearly proportional to $\delta$ within the range of $|\delta| \leqslant 0.3$ considered here. Such DBs are highly mobile. We have checked that they move through the entire computational cell of 4000 particles with nearly constant velocity and

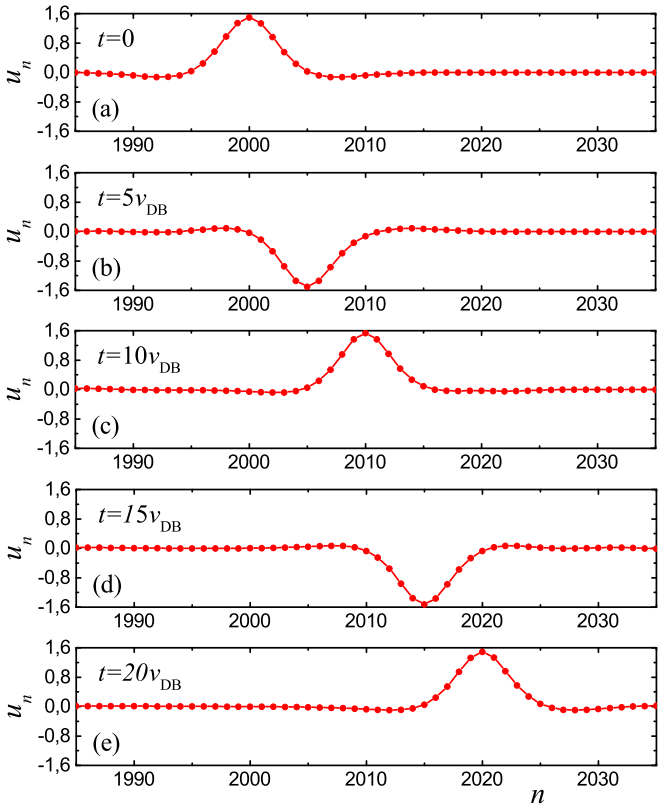


FIG. 13. Moving DB profile in the case of soft-type anharmonicity. Parameters of the ansatz Eq. (23) are $A_{\rm DB} = 1.5$, $\theta = 0.361$, $\omega_{\rm DB} = 0.932$, $x_0 = 2000$, $\delta = 0.3$. DB velocity $v_{\rm DB} = 0.2838$. Time is indicated in each panel.

practically radiating no energy. However, for the cases of $A_{\rm DB} = 2.5$, the increase of DB velocity with $\delta$ is slower than that for smaller amplitudes. While propagating, it radiates small-amplitude waves and its velocity gradually decreases.

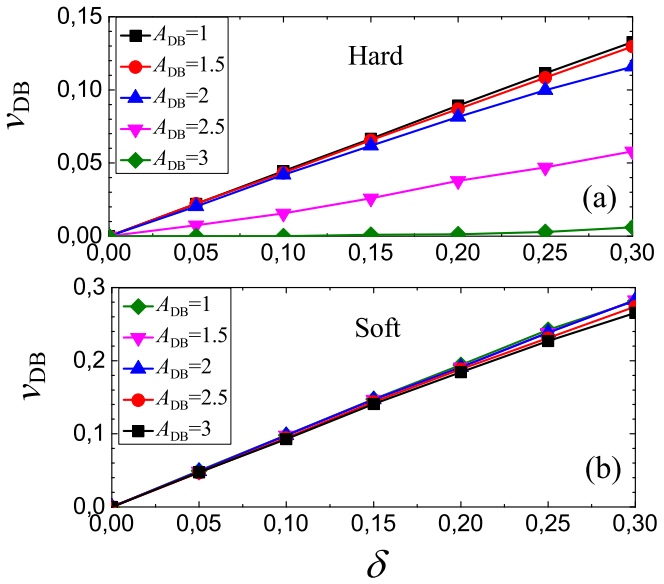


FIG. 14. Velocity $v_{\rm DB}$ of DBs as a function of $\delta$ for (a) hard-type and (b) soft-type anharmonicities. DB amplitude is indicated in the legends. Other DB parameters are taken from Table I.

For this reason, we measured the DB velocity at $t = 300$. Finally, DBs with even higher amplitudes ($A_{\rm DB} \geqslant 3$) are trapped by the lattice and no longer move for any value of $\delta$. On the other hand, as evidenced by Fig. 14(b), DBs in the lattice with soft-type anharmonicity are highly mobile for all the considered amplitudes up to $A_{\rm DB} = 3$.

### C. Analytical treatment

In fact, for the soft-type anharmonicity, the on-site potential Eq. (3) is a Taylor series expansion of $1 - \cos\xi$ up to the sixth-order term. In this sense, for not very large displacements, Eqs. (4) can be approximated by the Frenkel-Kontorova model [57]

$$m\ddot{u}_n = K(u_{n-1} - 2u_n + u_{n+1}) - \sin(u_n). \tag{24}$$

This model reduces to the sine-Gordon equation

$$u_{tt} - u_{xx} + \sin u = 0 \tag{25}$$

in the continuum limit ($K \to \infty$), where $x$ is a continuous variable corresponding to $n$ and $u(x,t)$ is a slowly varying function of $x$ and $t$. Then the well-known moving breather solution of Eq. (24) [58] has the form

$$u_n(t) = 4\arctan\frac{\eta\cos[\zeta\omega_{\rm DB}(t - v_{\rm DB}n)]}{\omega_{\rm DB}\cosh[\zeta\eta(n - v_{\rm DB}t)]} \tag{26}$$

after the substitutions of $x \to n$ and $u(x,t) \to u_n(t)$, where

$$\eta = \sqrt{1 - \omega_{\rm DB}^2}, \quad \zeta = \frac{1}{\sqrt{1 - v_{\rm DB}^2}}. \tag{27}$$

In a comparison of the solution Eq. (26) with our ansatz Eq. (23), one then derives the following relations for the DB parameters:

$$A_{\rm DB} = 4\arctan\frac{\eta}{\omega_{\rm DB}}, \tag{28}$$

$$\theta = \zeta\eta, \tag{29}$$

$$\delta = v_{\rm DB}\zeta\omega_{\rm DB}. \tag{30}$$

With this in mind, we also recall another analytical solution suggested by Ref. [14]; i.e., for small-amplitude breathers, one can resort to the nonlinear Schrödinger equation, from which analytical solutions for moving solitons (so, correspond to moving DBs) are available. Based on this, for the hard-type anharmonicity, one might find

$$u_n(t) = \frac{(-1)^n A_{\rm DB}\cos[\omega_{\rm DB}t + \omega_{\max}v_{\rm DB}n]}{\cosh[\theta(n - v_{\rm DB}t)]},$$
$$\theta = \sqrt{2\omega_{\max}\Omega + \omega_{\max}^2 v_{\rm DB}^2},$$
$$A_{\rm DB} = 4\theta, \quad \omega_{\rm DB} = \omega_{\max} + \Omega, \tag{31}$$

and for the soft-type anharmonicity, one obtains

$$u_n(t) = \frac{A_{\rm DB}\cos[\omega_{\rm DB}t - \omega_{\min}v_{\rm DB}n]}{\cosh[\theta(n - v_{\rm DB}t)]},$$
$$\theta = \sqrt{2\omega_{\min}\Omega + \omega_{\min}^2 v_{\rm DB}^2},$$
$$A_{\rm DB} = 4\theta, \quad \omega_{\rm DB} = \omega_{\min} - \Omega. \tag{32}$$

Here $\Omega > 0$ is a frequency parameter.

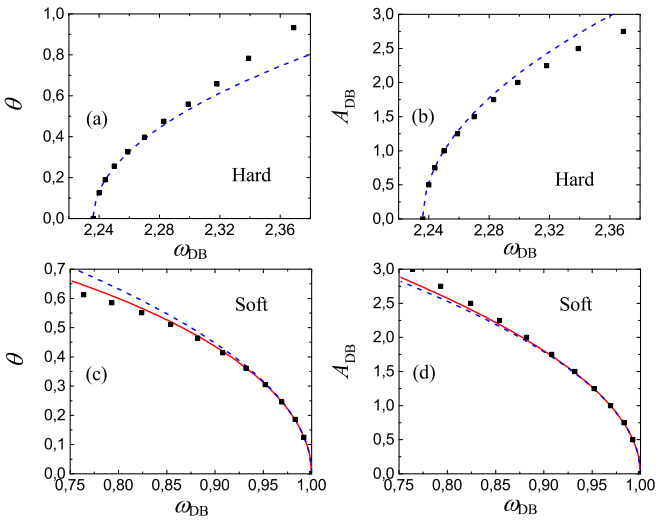


FIG. 15. $\theta$ and $A_{DB}$ as functions of $\omega_{DB}$ for standing DB for hard-type [(a), (b)] and soft-type [(c), (d)] anharmonicities, where the dots give the numerical estimates shown in Table I, the solid lines correspond to the solutions of the sine-Gordon breather, i.e., Eqs. (28) and (29), and the dashed lines are the solutions from Eqs. (31) and (32).

Viewing the above analytical results, in Fig. 15 we plot both DB inverse width $\theta$ and amplitude $A_{DB}$ as functions of DB frequency $\omega_{DB}$, for the standing DBs, for the hard- [Figs. 15(a) and 15(b)] and soft-type [Figs. 15(c) and 15(d)] anharmonicities, respectively. Here, the scattered symbols give numerical results presented in Table I, the solid lines in Figs. 15(a) and 15(b) correspond to the solution of the sine-Gordon breather from Eqs. (28) and (29), and the dashed lines are the solutions of Eq. (31) and Eq. (32). As can be seen, both analytical solutions are in good agreement with the numerical estimate for $A_{DB} < 1.5$, while we should note that the accuracy of the sine-Gordon breather solution is somewhat higher since it considers not only the quartic term of the on-site potential Eq. (3) but also its sixth-order term.

For the moving DB, in the case of soft-type anharmonicity, we find that, based on Eqs. (28), (29), and (30), when $A_{DB}$ is small, $\omega_{DB} \approx 1$, and for small $v_{DB}$, $v_{DB} \approx \delta$. Both are consistent with the numerical estimates in Fig. 14(b). The same conclusions can be drawn from Eq. (32), e.g., $v_{DB} = \delta/\omega_{min} = \delta$.

For the hard-type anharmonicity, from Eq. (31) one has $v_{DB} = \delta/\omega_{max} \approx 0.447\delta$, which also agrees well with the numerical estimates in Fig. 14(a) for the small-amplitude DB when its velocity is not very high.

### D. Relating DBs to energy transfer

With all of the above information, now we relate the energy transfer process due to the ac driving to properties of moving DBs. As was already mentioned in Sec. III B, DBs emitted by the driven particle at driving amplitude $A = 0.6$ have amplitudes about $A_{DB} = 1.1$ for both hard- and soft-type anharmonicities [see dashed lines in Figs. 9(b) and 9(c), respectively]. The velocity of DBs emitted by the driven particle at driving amplitude $A = 0.6$ can be estimated from Figs. 7(b′) and 7(c′) for hard- and soft-type anharmonicities, respectively, and they are found to be about 0.12 and 0.23, respectively. For the soft-type anharmonicity, the measured DB oscillation period gives a value around $T = 0.93$, which suggests a DB frequency of about $\omega_{DB} = 2\pi\zeta/T = 0.96$ [59]. For the hard-type anharmonicity the counterpart is about $\omega_{DB} = 2.25$. All of these show good agreement with both the numerical estimate in Table I and the analytical results shown in Fig. 15.

Due to all of these consistencies, one then might come to the following conclusion: the moving localized excitations emerging from the ac driven particle do show the properties, e.g., both amplitude and frequency, similarly to DBs. This relation thus supports our conjecture that moving DBs are responsible for the enhancement of energy transfer to the chain from the driven particle.

## V. CONCLUSIONS

Two typical chains of harmonically coupled particles placed in the sixth-order polynomial on-site potentials of hard-type and soft-type anharmonicities have been analyzed. First, energy transfer to the chain from one harmonically driven particle was analyzed for different driving amplitudes and for two driving frequencies within the phonon band and close to the upper and lower edges of the band. Second, properties of discrete breathers (DBs) were studied.

Our main findings are summarized as follows:

(1) An exact solution for the power of the energy source in the form of one particle moving according to the harmonic law with amplitude $A$ and frequency $\omega$ in a harmonic chain has been obtained; see Eq. (14). From this solution, the power of the energy source increases proportionally to $A^2$. For large times, the power of the energy source normalized to $A^2$ is proportional to $\omega^2$ and proportional to the group velocity of phonons with frequency $\omega$. This means that the power at large times vanishes for driving frequencies at the edges of the phonon band, where phonon group velocity vanishes.

(2) For the considered nonlinear models, driving with the amplitude $A \leqslant 0.2$ can be described by the linear theory quite well. For driving amplitudes $A > 0.4$, the effect of anharmonicity should be taken into account.

(3) When driving frequency is far from the DB frequency and close to the edge of the phonon spectrum, increase in the driving amplitude results in the reduction of the power, and as time increases, the power of the energy source approaches a constant value; see Fig. 5(a) and Fig. 6(b).

(4) When the driving frequency is close to the DB frequency and also close to the edge of the phonon spectrum, increase in the driving amplitude results in the increase of the power, and the power oscillates with time quasiperiodically; see Fig. 5(b) and Fig. 6(a). These oscillations reflect the emission of DBs moving away from the energy source; see Fig. 8(b) and 8(c). In the previous works [2,3,10,12–14], emission of DBs by driving with frequencies *outside* the phonon band was reported, but here we demonstrate that they can also be excited with driving frequencies *inside* the phonon band close to the DB frequency.

Overall, we have demonstrated that in the case of moderate driving amplitudes and driving frequencies close to the edges of the phonon band (within the band), DBs enhance energy transfer to the chain from the harmonically driven particle. This result contributes to our understanding of dynamics of nonlinear chains under external driving and uncovers the role of DBs in such systems.

## ACKNOWLEDGMENTS

We thank the referees for many helpful suggestions, in particular for the kind reminder of the analytical solution in [14]. The stay of D.S. at IMSP RAS was partly supported by the Russian Science Foundation, Grant No. 14-13-00982. The work of D.X. was supported by the National Natural Science Foundation of China (Grant No. 11575046), the Natural Science Foundation of Fujian Province, China (Grant No. 2017J06002), and the Qishan Scholar Research Fund of Fuzhou University, China. The work of V.A.K. was supported by the Russian Science Foundation (RSCF Grant No. 17-71-10213). The work of A.M.K. was supported by the Russian Foundation for Basic Research (RFBR Grant No. 16-29-15121). S.V.D. was supported by the Russian Science Foundation, Grant No. 16-12-10175. For S.V.D. this research was also supported by "The Tomsk State University competitiveness improvement programme".

[1] T. Rössler and J. B. Page, Phys. Rev. B **62**, 11460 (2000).
[2] F. Geniet and J. Leon, Phys. Rev. Lett. **89**, 134102 (2002).
[3] P. G. Kevrekidis, S. V. Dmitriev, S. Takeno, A. R. Bishop, and E. C. Aifantis, Phys. Rev. E **70**, 066627 (2004).
[4] J.-S. Wang, N. Zeng, J. Wang, and C. K. Gan, Phys. Rev. E **75**, 061128 (2007).
[5] N. Li, F. Zhan, P. Hanggi, and B. Li, Phys. Rev. E **80**, 011125 (2009).
[6] M. Johansson, G. Kopidakis, S. Lepri, and S. Aubry, Europhys. Lett. **86**, 10009 (2009).
[7] B.-Q. Ai, D. He, and B. Hu, Phys. Rev. E **81**, 031124 (2010).
[8] N. Beraha, A. Soba, R. Barreto, and M. F. Carusela, Physica A **433**, 9 (2015).
[9] M. I. Sena-Junior, L. R. F. Lima, and C. H. Lewenkopf, J. Phys. A: Math. Theor. **50**, 435202 (2017).
[10] I. Evazzade, I. P. Lobzenko, E. A. Korznikova, I. A. Ovid'ko, M. R. Roknabadi, and S. V. Dmitriev, Phys. Rev. B **95**, 035423 (2017).
[11] E. Barani, I. P. Lobzenko, E. A. Korznikova, E. G. Soboleva, S. V. Dmitriev, K. Zhou, and A. M. Marjaneh, Eur. Phys. J. B **90**, 38 (2017).
[12] I. Aranson, B. Meerson, and T. Tajima, Phys. Rev. A **45**, 7500 (1992).
[13] J.-G. Caputo, J. Leon, and A. Spire, Phys. Lett. A **283**, 129 (2001).
[14] R. Khomeriki, S. Lepri, and S. Ruffo, Phys. Rev. E **70**, 066626 (2004).
[15] A. S. Dolgov, Sov. Phys. Solid State **28**, 907 (1986).
[16] A. J. Sievers and S. Takeno, Phys. Rev. Lett. **61**, 970 (1988).
[17] S. Flach and C. R. Willis, Phys. Rep. **295**, 181 (1998).
[18] S. Flach and A. V. Gorbach, Phys. Rep. **467**, 1 (2008).
[19] S. V. Dmitriev, E. A. Korznikova, Yu. A. Baimova, and M. G. Velarde, Phys. Usp. **59**, 446 (2016).
[20] N. Li, J. Ren, L. Wang, G. Zhang, P. Hanggi, and B. Li, Rev. Mod. Phys. **84**, 1045 (2012).
[21] M. Madovan, Nature (London) **503**, 209 (2013).
[22] S. Lepri, R. Livi, and A. Politi, Phys. Rep. **377**, 1 (2003).
[23] A. Dhar, Adv. Phys. **57**, 457 (2008).
[24] C.-W. Chang, in *Thermal Transport in Low Dimensions*, Lecture Notes in Physics, Vol. 921 (Springer, London, 2016), p. 305.
[25] V. Lee, C.-H. Wu, Z.-X. Lou, W.-L. Lee, and C.-W. Chang, Phys. Rev. Lett. **118**, 135901 (2017).
[26] T.-K. Hsiao, B.-W. Huang, H.-K. Chang, S.-C. Liou, M.-W. Chu, S.-C. Lee, and C.-W. Chang, Phys. Rev. B **91**, 035406 (2015).
[27] T.-K. Hsiao, H.-K. Chang, S.-C. Liou, M.-W. Chu, S.-C. Lee, and C.-W. Chang, Nat. Nanotechnol. **8**, 534 (2013).
[28] J. Lee, J. Lim, and P. Yang, Nano Lett. **15**, 3273 (2015).
[29] Y. R. Koh, M. Shirazi-HD, B. Vermeersch, A. M. S. Mohammed, J. Shao, G. Pernot, J.-H. Bahk, M. J. Manfra, and A. Shakouri, Appl. Phys. Lett. **109**, 243107 (2016).
[30] D. Xiong, Phys. Rev. E **95**, 042127 (2017).
[31] D. Xiong, Europhys. Lett. **113**, 14002 (2016).
[32] B. Li, L. Wang, and G. Casati, Phys. Rev. Lett. **93**, 184301 (2004).
[33] B. Liu, J. A. Baimova, C. D. Reddy, S. V. Dmitriev, W. K. Law, X. Q. Feng, and K. Zhou, Carbon **79**, 236 (2014).
[34] B. Liu, C. D. Reddy, J. Jiang, H. Zhu, J. A. Baimova, S. V. Dmitriev, and K. Zhou, J. Phys. D: Appl. Phys. **47**, 165301 (2014).
[35] S. Hu, M. An, N. Yang, and B. Li, Small **13**, 1602726 (2017).
[36] Z. Duan, D. Liu, G. Zhang, Q. Li, C. Liu, and S. Fan, Nanoscale **9**, 3133 (2017).
[37] B. Li, L. Wang, and G. Casati, Appl. Phys. Lett. **88**, 143501 (2006).
[38] K. Joulain, J. Drevillon, Y. Ezzahri, and J. Ordonez-Miranda, Phys. Rev. Lett. **116**, 200601 (2016).
[39] L. Wang and B. Li, Phys. Rev. Lett. **99**, 177208 (2007).
[40] A. Fornieri, C. Blanc, R. Bosisio, S. D'Ambrosio, and F. Giazotto, Nat. Nanotechnol. **11**, 258 (2016).
[41] S. Murad and I. K. Puri, Appl. Phys. Lett. **102**, 193109 (2013).
[42] D. Xiong and J. Zhang, Letters on Materials **6**, 27 (2016).
[43] D. Xiong, D. Saadatmand, and S. V. Dmitriev, Phys. Rev. E **96**, 042109 (2017).
[44] T. Jin, J. Yu, N. Zhang, and H. Zhao, Phys. Rev. E **96**, 022116 (2017).
[45] A. V. Savin, Y. S. Kivshar, and B. Hu, Phys. Rev. B **82**, 195422 (2010).
[46] A. A. Le-Zakharov and A. M. Krivtsov, Dokl. Phys. **53**, 261 (2008).
[47] A. V. Savin and Y. A. Kosevich, Phys. Rev. E **89**, 032102 (2014).
[48] A. V. Savin and Yu. S. Kivshar, Phys. Rev. B **96**, 064307 (2017).
[49] K. V. Kepesidis, S. D. Bennett, S. Portolan, M. D. Lukin, and P. Rabl, Phys. Rev. B **88**, 064105 (2013).
[50] K. V. Kepesidis, M.-A. Lemonde, A. Norambuena, J. R. Maze, and P. Rabl, Phys. Rev. B **94**, 214115 (2016).

[51] A. M. Krivtsov, Dokl. Phys. **60**, 407 (2015).
[52] V. A. Kuzkin and A. M. Krivtsov, Dokl. Phys. **62**, 85 (2017).
[53] V. A. Kuzkin and A. M. Krivtsov, Phys. Solid State **59**, 1051 (2017).
[54] A. A. Sokolov, A. M. Krivtsov, and W. H. Müller, Phys. Mesomech. **20**, 305 (2017).
[55] V. A. Kuzkin and A. M. Krivtsov, J. Phys.: Condens. Matter **29**, 505401 (2017).
[56] A. A. Kistanov, R. T. Murzaev, S. V. Dmitriev, V. I. Dubinko, and V. V. Khizhnyakov, JETP Lett. **99**, 353 (2014).
[57] O. M. Braun and Yu. S. Kivshar, Phys. Rep. **306**, 1 (1998).
[58] R. K. Dodd, J. C. Eilbeck, J. D. Gibbon, and H. C. Morris, *Solitons and Nonlinear Wave Equations* (Academic Press, London, 1982).
[59] S. V. Dmitriev, T. Shigenari, A. A. Vasiliev, and A. E. Miroshnichenko, Phys. Lett. A **246**, 129 (1998).